Structure of the Maize Streak Virus Geminate Particle

Wei Zhang,* Norman H. Olson,* Timothy S. Baker,* Lee Faulkner,†,‡ Mavis Agbandje-McKenna,‡
Margaret I. Boulton,§ Jeffrey W. Davies,§ and Robert McKenna‡,1

*Department of Biological Sciences, Purdue University, West Lafayette, Indiana 47907-1392; †Department of Biological Sciences, University
of Warwick, Coventry CV4 7AL, United Kingdom; ‡Department of Biochemistry and Molecular Biology, College of Medicine,
Brain Institute, University of Florida, Gainesville, Florida 32610-0245; and §Department of Virus Research,
John Innes Centre, Norwich Research Park, Colney Lane, Norwich NR4 7UH, United Kingdom

The *Geminiviridae* is an extensive family of plant viruses responsible for economically devastating diseases in crops worldwide. Geminiviruses package circular, single-stranded DNA (ssDNA) genomes. The characteristic twinned or "geminate" particles, which consist of two joined, incomplete $T = 1$ icosahedra, are unique among viruses. We have determined the first structure of a geminivirus particle, the Nigerian strain of *Maize streak virus* (MSV-N), using cryo-electron microscopy and three-dimensional image reconstruction methods. The particle, of dimensions 220×380 Å, has an overall 52-point-group symmetry, in which each half particle "head" consists of the coat protein (CP) arranged with quasi-icosahedral symmetry. We have modeled the MSV-N CP as an eight-stranded, antiparallel β-barrel motif (a structural motif common to all known ssDNA viruses) with an N-terminal α-helix. This has produced a model of the geminate particle in which 110 copies of the CP nicely fit into the reconstructed density map. The reconstructed density map and MSV-N pseudo-atomic model demonstrate that the geminate particle has a stable, defined structure.   © 2001 Academic Press

Key Words: cryo-electron microscopy; Geminiviridae; icosahedral capsid; maize streak virus; ssDNA virus; three-dimensional image reconstruction.

INTRODUCTION

At the beginning of the twentieth century, a condition of maize described by Fuller (1901) as "mealie variegation" was recorded and later renamed "maize streak disease." This condition was subsequently shown to be caused by infection with *Maize streak virus* (MSV), a species of the genus *Mastrevirus* of the family *Geminiviridae* (Mayo and Pringle, 1997). This family of viruses, all of which contain single-stranded DNA (ssDNA) genomes, gained its name from the characteristic twinned (geminate) particle morphology of its members. Geminiviruses are agronomically important throughout the world (Lazarowitz, 1992). MSV, for example, causes major economic problems for subsistence farmers in sub-Saharan Africa where maize is a staple food (Palmer and Rybicki, 1997, 1998; Thottappilly *et al.,* 1993).

The Nigerian strain of MSV (MSV-N) packages a ssDNA genome of 2687 nucleotides (Mullineaux *et al.,* 1984) that encodes four gene products, which are conserved within the mastreviruses (Boulton *et al.,* 1989). The 244 amino acid residue V2, or coat protein (CP), is the only structural protein found in particles (Mullineaux *et al.,* 1988). The CP is multifunctional, in that it is required for encapsidation and accumulation of ssDNA

(Boulton *et al.,* 1993), insect transmission (Mullineaux *et al.,* 1984), transport of MSV DNA into the cell nucleus (Liu *et al.,* 1999), and systemic infection of maize plants (Boulton *et al.,* 1989; Lazarowitz *et al.,* 1989). Furthermore, the CP binds single- and double-stranded DNA (Liu *et al.,* 1997) and may interact with the virus-encoded movement protein to facilitate cell-to-cell spread of the virus (Liu, 1997; Pitaksutheepong, 1999).

As demonstrated in this study, the geminate MSV-N particle, with overall dimensions of 220×380 Å, consists of two joined, incomplete $T = 1$ icosahedral "heads," and a total of 110 CP subunits, organized as 22 pentameric capsomers. It is thought that *Mastrevirus* particles contain only one ssDNA molecule (Francki *et al.,* 1980). The *Geminiviridae* provide a novel system for studying the mechanism by which CPs and encapsidated genomes assemble to form a unique virus particle.

Here we report on a cryo-electron microscopy (cryo-EM) and three-dimensional image reconstruction study, which reveals the structure of frozen-hydrated MSV-N particles to 25-Å resolution. We also present an amino acid sequence alignment of the CP of MSV-N with the CP of the RNA virus, satellite tobacco necrosis virus (STNV), which made possible the building and fitting of a pseudo-atomic model of the CP of MSV-N into the cryo-EM density map. The clarity of features in the MSV-N reconstruction demonstrates that the "two-headed" *Geminiviridae* particles are uniform in shape

---

[1] To whom correspondence and reprint requests should be addressed. Fax: (352) 392-3422. E-mail: rmckenna@ufl.edu.
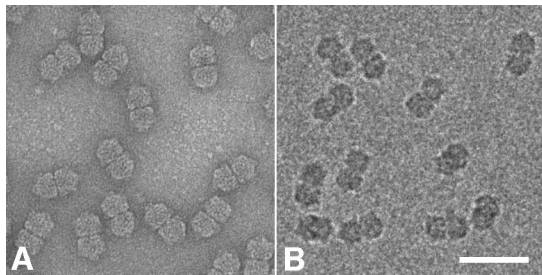
FIG. 1. Electron microscopy of MSV-N. Micrographs of MSV-N, negatively stained with 1% uranyl acetate (A) and vitrified in a thin layer of 0.1 M sodium acetate buffer, pH 4.8, recorded on a $1K^2$ slow-scan, CCD camera under low-dose conditions ($\sim$20 e$^-$/Å^2) and 0° tilt (B). The images show the two-headed particle morphology in a variety of orientations. The stained particles (A) are noticeably larger ($\sim$35% in width and 10% in length) than the vitrified particles (B) as a consequence of flattening that often occurs in particles when they are adhered to a support film in a thin layer of stain. In the micrographs the particles tended to align with their long axis, either perpendicular or at about 30° with respect to the electron beam. Scale bar = 500 Å.

and size and have a stable, defined morphology with a capsid consisting of two incomplete icosahedra and a total of 110 copies of the CP arranged with 52-point symmetry.

RESULTS AND DISCUSSION

Cryo-EM and three-dimensional image reconstruction

Negatively stained MSV-N particles exhibit the characteristic twinned-isometric morphology of geminiviruses (Fig. 1A). The particles adopt various orientations on the microscope grid and, from images of such samples, it is uncertain whether the capsids are uniform in shape and size or whether the heads are joined via flexible links. Careful examination of images of particles embedded in vitreous ice (Fig. 1B) and subsequent three-dimensional image reconstruction (Fig. 2) clearly demonstrate that MSV-N has a well-defined structure with specific connections that link the heads.

A simple geminivirus model, with 52-point-group symmetry (Fig. 2A), was first proposed by Hatta and Francki on the basis of their inspection of negatively stained virus particles (Hatta and Francki, 1979). Our MSV-N reconstruction confirmed this model and additionally reveals details of the quasi-icosahedral organization of the particle (Figs. 2C–2H). MSV-N consists of a pair of quasi-spherical heads, in which a fivefold symmetry axis coincides with the long axis of the particle. Each head con-
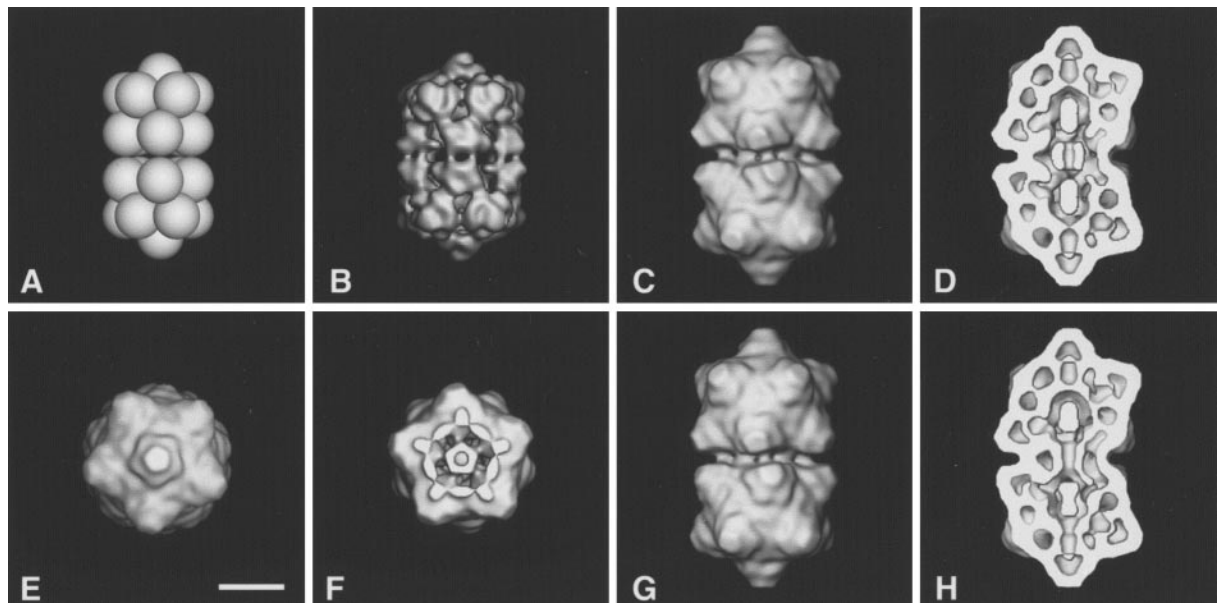

FIG. 2. Models and image reconstruction of MSV-N. (A) "Ping-pong" model (Hatta and Francki, 1979) for the capsid structure of gemini viruses, consisting of 22 "subunits" (capsomers), arranged with 52-point-group symmetry. (B) Surface-shaded, pseudo-atomic model of MSV-N based on the structure of STNV (Liljas and Jones, 1984), rendered at 25-Å resolution and used as an initial model for particle orientation refinement (see Materials and Methods). (C) MSV-N reconstruction computed with 52-dihedral-point-group symmetry and viewed along a twofold axis of symmetry. Handedness in the reconstruction is evident in the skewed disposition of capsomers near the equatorial region. The absolute hand of the MSV-N capsid was established by means of tilting experiments (data not shown) (Belnap *et al.,* 1997). The striking difference in size of the initial model (195 × 305 Å) compared with that of the reconstruction (220 × 380 Å) provided a stringent test of the reliability of the reconstruction procedures because it demonstrated that the model was useful for generating initial estimates of particle orientation parameters, yet without introducing a bias into their refinement or the final result. (D) Same as (C) but with the nearest half of the reconstruction removed to expose the particle interior. (E) End-on-view of MSV-N reconstruction in which only fivefold axial symmetry was imposed during the processing. (F) Same as (E) but with one head removed to reveal features in the gap region. (G, H) Views of the reconstruction with just fivefold cyclic symmetry for comparison with corresponding views of the 52-symmetric reconstruction shown in (C) and (D). The nearly indistinguishable exteriors (C, G) strongly support the notion that the MSV-N capsid proteins are organized with 52-dihedral symmetry in the capsid. Minor asymmetry in the distribution of internal features as seen in (H) is presumably attributable to the genome organization inside MSV-N particles. The scale bar in (E) represents 100 Å in all panels.
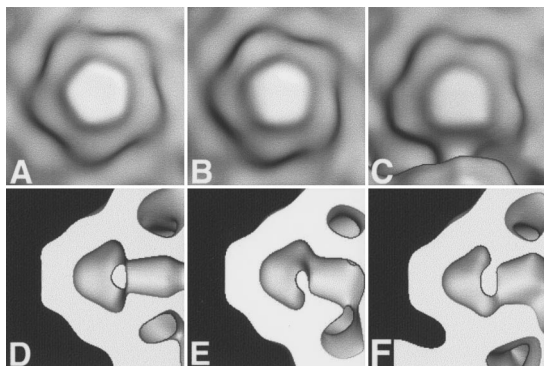
FIG. 3. Magnified axial (A, B, C) and cross-sectioned (D, E, F) views of the three types of capsomers from the MSV-N reconstruction computed with fivefold cyclic symmetry. (A, D) An apical capsomer with strict fivefold symmetry imposed by the reconstruction process. (B, E) A peripentonal capsomer, which exhibits good, local fivefold symmetry. (C, F) An equatorial capsomer, which exhibits distortion in the CP closest to the particle gap. The cross-sectional views (D–F) show that all three capsomer types are dome-shaped structures with a conical cavity inside the particle.

tains 11 pentameric capsomers and each capsomer has five CPs. The apical capsomers, at the two ends of the particle, exhibit strict fivefold symmetry as imposed in the reconstruction protocol (Figs. 3A and 3D). Five peripentonal capsomers contact each of the apical capsomers and each of the 10 capsomers of this type display intrinsic, local fivefold symmetry (Figs. 3B and 3E). The remaining 10 capsomers, near the equatorial region of the particle, are distorted pentamers (Figs. 3C and 3F). Associated with these pentamers are two sets of five symmetrically equivalent cylinders of density, arranged in inner and outer rings, that form 10 connections and span a 25-Å gap between the two heads of the particle (Figs. 2C, 2D, 2G, and 2H).

Pseudo-atomic model building and fit to the cryo-EM density map

A pseudo-atomic model of the MSV-N CP was built based on a structural alignment (Fig. 4A) with the atomic coordinates (Fig. 4B) of the CP of STNV (Liljas and Jones, 1984). The structure of the CP of STNV was used as the framework onto which the MSV-N sequence was fit because it exhibits the highest score in segment pairing with MSV-N as computed with a BLAST network search, although other virus β-barrel structures were listed (Gish, 1999). The β-barrel motif is a dominant, unifying motif in all ssDNA virus structures that have been determined to atomic resolution (Agbandje et al., 1993; Agbandje-McKenna et al., 1998; McKenna et al., 1992, 1996; Simpson et al., 1998; Tsao et al., 1991). The MSV-N and STNV CPs share 18% sequence identity that is comparable to levels previously reported by Rao (1986). The percentage of identical residues for the pairwise structural alignment between the two CPs shows a slight

increase in conservational pressure for the eight β-strands, 21% (20 out 95 residues), compared to all other residues within the CP, 15% (23 out of 149 residues). This observation is a direct consequence of producing the maximal pairwise agreement between the two CPs, and all the additional residues found in the CP of MSV-N compared to STNV occur in the insertion loops between the β-strands. Hence, the modeled β-barrel motif of the MSV-N CP contains additional amino acid residues compared to that of STNV and these are at the corners of the B−C (IN5), D−E (IN6), F−G (IN8), and H−I (IN11) β-strands (Fig. 4A).

All these insertion loops point toward the local fivefold axes of the capsomers (Fig. 5A). Clashes among these additional amino acid residues at intracapsomer interfaces compared to the STNV CPs were prevented by radially and tangentially translating the MSV-N CPs about the fivefold axes, using simple computer programs that maintained icosahedral symmetry, which resulted in a 15.4-Å translation of the MSV-N CPs compared to that of an STNV particle. This adjustment led to a 31-Å expansion of the diameter of each head when compared to that of a geminate particle generated using the STNV CP structure alone (Fig. 2B). The resulting model was found to be consistent with the dimensions of the MSV-N reconstruction (Fig. 2C). Additional insertions (IN7, IN9, and IN10 in Figs. 4A and 5A) were clustered at the intercapsomer interfaces (at local twofold positions).

In the STNV CP structure (Liljas and Jones, 1984), the N-terminal region is ordered after residue 12 (residue 18 of the CP of MSV-N) and forms an α-helix structure. We examined the first 18 amino acids of the CP of MSV-N (which contains five lysine and three arginine residues) in a BLAST network search (Gish, 1999) and found eight of the top 10 highest-scoring segment pairings to have sequences with known α-helical structure (data not shown). Hence, we modeled the N-terminal sequence of the CP of MSV-N as an α-helix based on its structural alignment with the STNV CP (Fig. 4A) and knowledge of the residues. To better fit the reconstructed density map, the modeled N-terminal α-helix was rotated through a single backbone torsion angle (75° around the Cα of residue 35 in IN4). This positioned the helix in a tangential orientation quite distinct from the radial position occurring in the STNV CP crystal structure (Figs. 4B and 4C). For the CPs comprising each apical capsomer (Figs. 3A, 3D, and 5A) and the CPs from the peripentonal capsomers that contact the apical capsomers (Figs. 3B, 3E, and 5A), three CP α-helices converge at the local threefold axes and maintain icosahedral symmetry (Figs. 5A and 5B). In each of the remaining 10 equatorial capsomers, four of the five CPs adopt a conformation similar to that observed in the CPs of the apical and peripentonal capsomers.

Because the conformation of the unique CP differs significantly from the other CPs, the modeled N-terminal
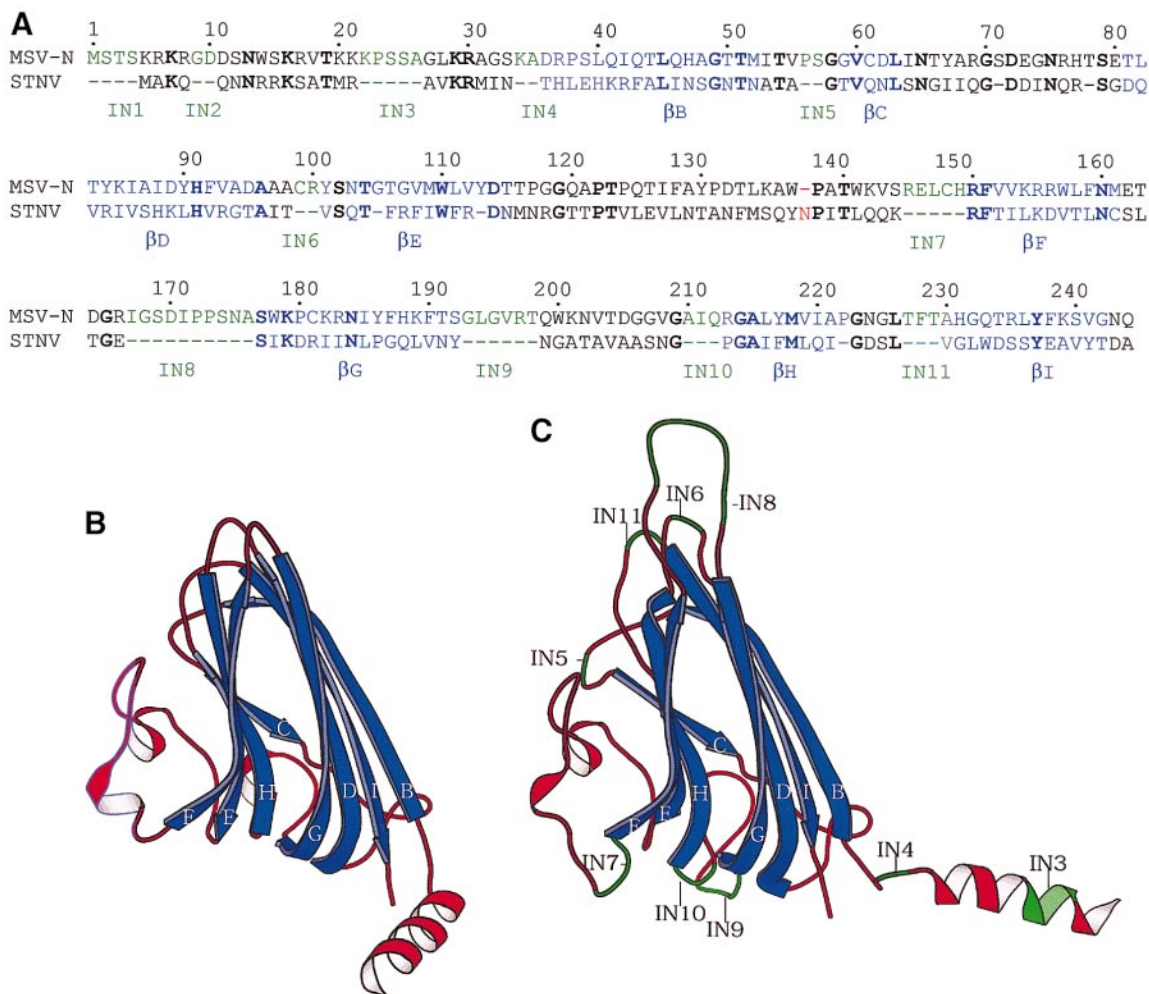
A

```
        1         10        20        30        40        50        60        70        80
        .         .         .         .         .         .         .         .         .
MSV-N   MSTSKRKRGDDSNWSKRVTKKKPSSAGLKRAGSKADRPSLQIQTLQHAGTTMITVPSGGVCDLINTYARGSDEGNRHTSETL
STNV    ----MAKQ--QNNRRKSATMR-----AVKRMIN--THLEHKRFALINSGNTNATA--GTVQNLSNGIIQG-DDINQR-SGDQ
           IN1   IN2               IN3       IN4       βB        IN5  βC

                  90        100       110       120       130       140       150       160
                  .         .         .         .         .         .         .         .
MSV-N   TYKIAIDYHFVADAAACRYSNTGTGVMWLVYDTTPGGQAPTPQTIFAYPDTLKAW-PATWKVSRELCHRFVVKRRWLFNMET
STNV    VRIVSHKLHVRGTAIT--VSQT-FRFIWFR-DNMNRGTTPTVLEVLNTANFMSQYNPITLQQK-----RFTILKDVTLNCSL
             βD        IN6      βE                                       IN7      βF

                  170       180       190       200       210       220       230       240
                  .         .         .         .         .         .         .         .
MSV-N   DGRIGSDIPPSNASWKPCKRNIYFHKFTSGLGVRTQWKNVTDGGVGAIQRGALYMVIAPGNGLTFTAHGQTRLYFKSVGNQ
STNV    TGE---------SIKDRIINLPGQLVNY------NGATAVAASNG---PGAIFMLQI-GDSL---VGLWDSSYEAVYTDA
             IN8       βG        IN9            IN10  βH          IN11    βI
```


FIG. 4. Sequence alignment and model of the MSV-N coat protein. (A) Pairwise sequence alignment of the CP sequences of MSV-N and STNV. Residue numbering is based on the MSV-N sequence. Identical residues are bold. Residues in the β-strands are colored blue. Sequences in the MSV-N CP with no equivalent in STNV (insertions) are colored green. Insertions of more than two amino acids are labeled IN1 to IN11. A deleted residue not present in MSV-N CP compared to STNV is colored red. Ribbon drawing of the CPs of STNV (B) and MSV-N (C) in which the β-barrel motif (blue) has the β-strands labeled according to convention (B, I, D, G and C, H, E, F). IN3 to IN11 are depicted in green.

α-helix in this CP was rotated through the same single backbone torsion angle (70° around the Cα of residue 35 in IN4), but to a different position found in the other CPs. In this conformation these α-helices form end-to-end contacts and satisfy the electron density of the five symmetrically equivalent cylinders that form the inner ring of connections and span the 25-Å gap between the two heads of the particle (Figs. 5A and 5C). However, no part of the current CP model is ascribed to the five outer cylindrical density features (Fig. 5D). Attempts to model the N-terminal α-helices (Fig. 4C) into this density, based on simple backbone conformational torsion angles, were unsuccessful. Thus, these connections may represent ordered regions of genomic ssDNA or, more likely, they result from complex conformational changes in the N-terminal α-helix of the distorted CPs (Figs. 3C and 3F). At the current level of resolution, the reconstruction does not permit accurate modeling of this distorted part of the

CP structure. The N-terminal 20 residues of the MSV-N CP are involved in binding the genomic DNA (Liu *et al.,* 1997). Distortion of the equatorial capsomers may thus be affected by DNA–CP interactions. A model of MSV-N in which DNA–CP interactions are critical for CP organization is consistent with the observation that geminate particles have thus far only been observed assembled with their genomic ssDNA (Francki *et al.,* 1980). Our model suggests that the N-terminal α-helices of the CPs are involved in conformational switching, determined by their location in the particle, and also, perhaps, by interactions with the genome. A central role for the N-terminal α-helix in maintaining the geminate particle architecture is consistent with the known association of this region of amino acids with particle assembly and DNA recognition.

Visual comparison of the pseudo-atomic model of MSV-N and the image reconstruction reveals a close
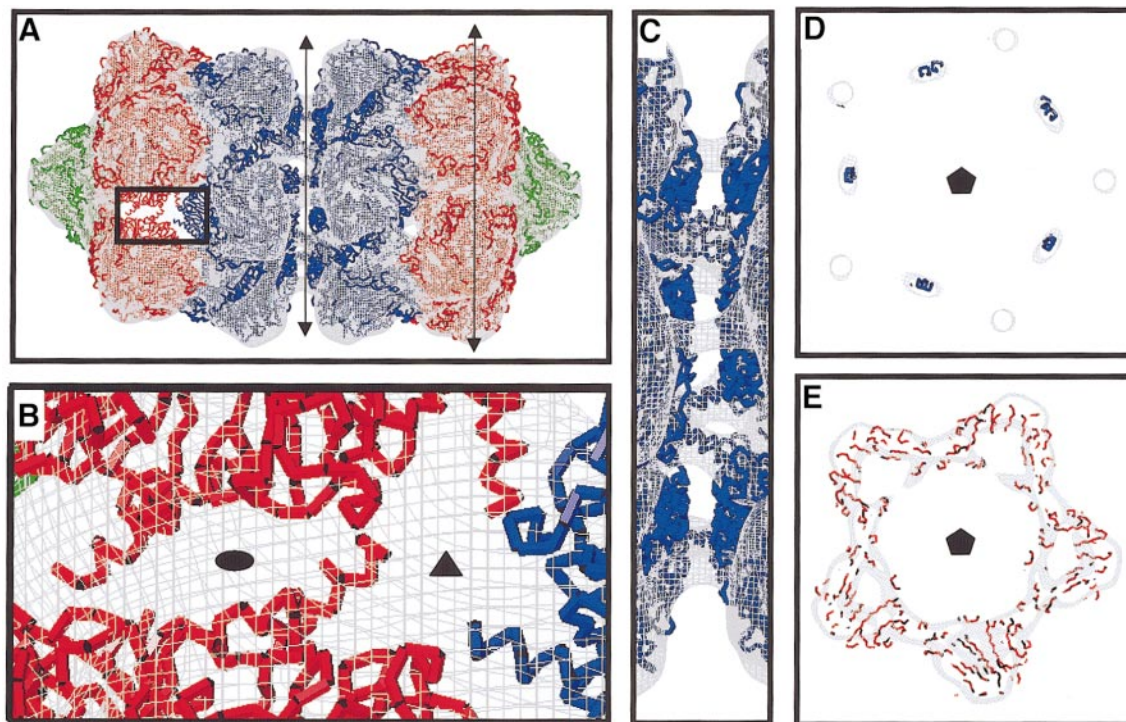
FIG. 5. Fit of the MSV-N coat protein pseudo-atomic model into the reconstruction density map of the MSV-N particle (gray isodensity contour). (A) Fit of 110 copies of the CPs (Cα tracings), the two apical capsomers, 10 peripentonal capsomers, and 10 equatorial capsomers shown in green, red, and blue, respectively. The rectangular boxed region indicates the position of the close-up view of the model fit shown in (B) of the two- and threefold icosahedral interactions. The double-ended arrow at the equatorial region indicates the position of the close-up view shown in (C) of the equatorial capsomer interactions and the cross-sectional slice of the MSV-N particle shown in (D). The double-ended arrow through the peripentonal capsomers on the right-hand-side of the particle indicates the position of the cross-sectional slice shown in (E). The icosahedral two-, three-, and fivefold axes are indicated as black ellipsoids, triangles, and pentamers, respectively.

correspondence (Figs. 5A, 5B, and 5E), with the exception of the outer ring of five connections at the equator (Figs. 5C and 5D). More precise modeling requires analysis of the MSV-N structure at higher resolution, which might be aided by the occasional presence of paracrystalline, two-dimensional arrays of MSV in vitrified samples (data not shown). The available data on the genetic variability of MSV strains (Briddon *et al.,* 1994) and *Mastreviruses* in combination with this model will enable preliminary structural mapping of the multifunctional regions and properties of the CP (Boulton *et al.,* 1989, 1993; Lazarowitz *et al.,* 1989; Liu *et al.,* 1999; Mullineaux *et al.,* 1984). This will further elucidate the roles of the CP in the life cycle of Geminiviruses.

Structural studies of the MSV-N particle provide an opportunity to better understand the principles by which geminate particles assemble. Such studies will also permit the multifunctional roles of the CP to be mapped within the structure, which ultimately can aid in the development of virus control procedures.

MATERIALS AND METHODS

Isolation and purification of MSV-N

Maize plants were agroinoculated with the Nigerian strain of MSV as previously described (Boulton *et al.,* 1989). Symptomatic leaves were harvested between 18 and 25 days postinoculation. Infected tissue was cut into 2- to 3-cm lengths, rapidly frozen, and stored at −20°C. Partially purified virus was obtained from tissue as previously described (Pinner *et al.,* 1988). The resultant pellet was resuspended in a minimum volume of 0.1 M sodium acetate buffer (pH 4.8), loaded onto a 10–40% sucrose gradient, and centrifuged in an SW41Ti rotor (Beckman Instruments, Fullerton, CA) at 160,000 *g* for 3 h. The fraction containing virus particles was dialyzed against 0.1 M sodium acetate buffer (pH 4.8) and the virus concentration was adjusted to 1 mg/ml (using an extinction coefficient of 7.5 mg/ml per cm at 260 nm). A total of 2–3 mg of virus was typically harvested from 100 g of infected plant tissue.

Negative stain, cryo-electron microscopy, and image reconstruction

Small aliquots (∼2 μl) of MSV-N samples were negatively stained with 1% uranyl acetate on a carbon support film and observed in a Philips EM420 electron microscope at a nominal magnification of 49,000×. For cryo-EM, 3.5-μl aliquots of MSV-N sample were prepared as described (Baker *et al.,* 1999). Vitrified virus samples were maintained at −185°C in a Gatan Model 626 cryo-

holder and images were recorded between 1.6 and 1.9 μm underfocus on Kodak SO-163 film in a Philips CM200 FEG transmission electron microscope under low-dose conditions ($\sim$20 e$^-$/Å^2) at 38,000× nominal magnification (Fig. 1).

Eleven micrographs of MSV-N were selected for processing on the basis of their displaying uniform sample thickness and distribution of virus particles, and exhibiting minimal drift and astigmatism as determined from the averaged particle image Fourier transforms (Zhou et al., 1996). These micrographs were digitized with a Zeiss-SCAI scanner at 7-μm intervals, which corresponds to 1.84-Å spacings in the specimen. The digitized data were either used directly or bin-averaged to give 3.68-Å pixels. A total of 2146 MSV-N particle images were boxed and floated (Baker et al., 1999) and then preprocessed to remove linear background gradients (Booy et al., 1991). The mean intensity and variance for each particle image were normalized for the entire data set (Carrascosa and Steven, 1978).

As a result of the elongated morphology of MSV-N particles, a modified strategy for determining and refining the particle orientations and origins was adapted from the model-based procedures that are routinely used to study images of icosahedral particles (Baker and Cheng, 1996; Baker et al., 1999; Fuller et al., 1996). A starting model, used to help generate initial estimates of each particle orientation (Θ, Φ, Ω) and center (x, y), was built from 22 pentamers of the coat protein of STNV (Liljas and Jones, 1984), arranged according to the simple model proposed by Hatta and Francki (1979) (Fig. 2A). The STNV pentamers in this model were arranged to give a 10-Å gap between the two incomplete icosahedra, consistent with images of negatively stained particles (Fig. 1A).

In our modified strategy for determining particle orientations, the angle Ω, the direction of the long axis, can be determined for elongated molecules quite accurately, especially for particles aligned with their axes within 45° of the plane of the EM grid (i.e., with Θ between 45 and 90°), without knowledge of the Θ and Φ angles. Hence, in this new procedure, Ω is estimated first for each individual particle image, then the Θ and Φ values are identified that lead to the best correlation coefficient between a projection of the starting model or current reconstruction and the particle image. Correlation coefficients are very sensitive to changes in Θ, especially for small values of Θ (particle in near-axial view) and the projected length of the particle varies rapidly. The orientation and the center of each particle were then gradually refined in cycles until convergence of these parameters was obtained. The final three-dimensional reconstruction was computed from 1516 particle images by means of Fourier–Bessel methods (Fuller et al., 1996) that were modified to allow imposition of either 52 dihedral or

fivefold cyclic point-group symmetries (Tao, Baker, and Belnap, unpublished data).

Reconstructions were computed without attempting to compensate for the effects of the contrast transfer function of the CM200 microscope (Baker et al., 1999). No data were used that extended beyond the first node of the transfer function for any micrograph. For these and other reasons (e.g., number of particle images, defocus settings of micrographs, orientations of particles in vitrified samples) the resolution of the final reconstructed density maps were limited to 25 Å, as assessed by calculating a reliability index that compares both amplitude and phase information between two reconstructions computed from independent sets of particle images (Baker et al., 1999). Although the long axis of the particles tended to adopt one of two preferred orientations, within the entire set of images the particle orientations were sufficiently distributed throughout the asymmetric unit such that all inverse eigenvalues were less than 0.01 (Fuller et al., 1996). Selection of the images used in the final reconstruction, from the 2146 total data set, was based on choosing those particles whose correlation coefficients (cc) were greater than 0.40. The average real-space cc, computed between model projections and the selected final 1516 images, was 0.485 $\pm$ 0.042.

Modeling of MSV-N CP and capsid

The CP amino acid sequences of several MSV strains (Briddon et al., 1994) were aligned to STNV (Liljas and Jones, 1984) using the pileup program (Devereux et al., 1984), with default gap penalties. A "working" model of the MSV-N CP structure was built using the program O (Jones et al., 1991) based on the atomic structure of the STNV CP (Liljas and Jones, 1984) and included minor adjustments to the final pairwise sequence alignment guided by the known secondary structural elements of STNV. The model was constrained using the structural geometry library of the program O (Jones et al., 1991). Because of the unusual particle symmetry of MSV (Hatta and Francki, 1979), 55 icosahedral symmetry operators were applied to generate one head (i.e., an incomplete icosahedral particle in which five CP subunits are missing), or half a geminate particle. The second head was generated from the first one by means of a twofold symmetry operation applied about an axis normal to the strict fivefold axis of the first head and positioned to create a 25-Å gap between the heads, as observed in the reconstructed density map. This procedure produced a model of the MSV-N particle consisting of 110 copies of the CP.

ACKNOWLEDGMENTS

REFERENCES

Agbandje, M., McKenna, R., Rossmann, M. G., Strassheim, M. L., and Parish, C. R. (1993). Structure determination of feline panleukopenia virus empty particles. *Proteins* **16,** 155–171.

Agbandje-McKenna, M., Llamas-Saiz, A. L., Wang, F., Tattersall, P., and Rossmann, M. G. (1998). Functional implications of the structure of the murine parvovirus, minute virus of mice. *Structure* **6,** 1369–1381.

Baker, T. S., and Cheng, R. H. (1996). A model-based approach for determining orientations of biological macromolecules imaged by cryoelectron microscopy. *J. Struct. Biol.* **116,** 120–130.

Baker, T. S., Olson, N. H., and Fuller, S. D. (1999). Adding the third dimension to virus life cycles: Three-dimensional reconstruction of icosahedral viruses from cryo-electron micrographs. *Microbiol. Mol. Biol. Rev.* **63,** 862–922.

Belnap, D. M., Olson, N. H., and Baker, T. S. (1997). A method for establishing the handedness of biological macromolecules. *J. Struct. Biol.* **120,** 44–51.

Booy, F. P., Newcomb, W. W., Trus, B. L., Brown, J. C., Baker, T. S., and Steven, A. C. (1991). Liquid-crystalline, phage-like packing of encapsidated DNA in herpes simplex virus. *Cell* **64,** 1007–1015.

Boulton, M. I., Steinkellner, H., Donson, J., Markham, P. G., King, D. I., and Davies, J. W. (1989). Mutational analysis of the virion-sense genes of maize streak virus. *J. Gen. Virol.* **70,** 2309–2323.

Boulton, M. I., Pallaghy, C. K., Chatani, M., MacFarlane, S., and Davies, J. W. (1993). Replication of maize streak virus mutants in maize protoplasts: Evidence for a movement protein. *Virology* **192,** 85–93.

Briddon, R. W., Lunness, P., Chamberlin, L. C. L., and Markham, P. G. (1994). Analysis of genetic variability of maize streak virus. *Virus Genes* **9,** 93–100.

Carrascosa, J. L., and Steven, A. C. (1978). A procedure for evaluation of significant structural differences between related arrays of protein molecules. *Micron* **9,** 199–206.

Devereux, J., Haeberli, P., and Smithies, O. (1984). A comprehensive set of sequence analysis programs for the VAX. *Nucleic Acids Res.* **12,** 387–395.

Francki, R. I. B., Hatta, T., Boccardo, G., and Randles, J. W. (1980). The composition of chloris striate mosaic virus, a geminivirus. *Virology* **101,** 233–241.

Fuller, C. (1901). Mealie variegation. First Reports of the Government Entomologist in Natal, 1899–1990. pp. 17–19.

Fuller, S. D., Butcher, S. J., Cheng, R. H., and Baker, T. S. (1996). Three-dimensional reconstruction of icosahedral particles: The uncommon line. *J. Struct. Biol.* **116,** 48–55.

Gish, W. (1996–1999) http://blast.wust1.edu.

Hatta, T., and Francki, R. I. B. (1979). The fine structure of Chloris striate mosaic virus. *Virology* **92,** 428–435.

Jones, T. A., Zou, J. Y., Cowan, S. W., and Kjedgaard, M. (1991). Improved methods from building protein models in electron-density maps and the location of errors in these models. *Acta Crystallogr. A* **47,** 110–119.

Lazarowitz, S. G. (1992). Geminiviruses: Genome structure and gene function. *Crit. Rev. Plant Sci.* **11,** 327–349.

Lazarowitz, S. G., Pinder, A. J., Damsteegt, V. D., and Rogers, S. G. (1989). Maize streak virus genes essential for systemic spread and symptom development. *EMBO J.* **8,** 1023–1032.

Liljas, L., and Jones, T. A. (1984). Structure of satellite tobacco necrosis virus after crystallographic refinement at 2.5Å resolution. *J. Mol. Biol.* **177,** 735–745.

Liu, H. (1997). Molecular biology of maize streak virus movement in maize. Ph.D. thesis, University of East Anglia, UK.

Liu, H., Boulton, M. I., and Davies, J. W. (1997). Maize streak virus coat protein binds single and double stranded DNA in vitro. *J. Gen. Virol.* **78,** 1265–1270.

Liu, H., Boulton, M. I., Thomas, C. L., Prior, D. A., Oparka, K. J., and Davies, J. W. (1999). Maize streak coat protein is karyophyllic and facilitates nuclear transport of viral DNA. *Mol. Plant–Microbe Interact.* **10,** 894–900.

Mayo, M. A., and Pringle, C. R. (1997). Virus taxonomy. *J. Gen. Virol.* **79,** 649–657.

McKenna, R., Bowman, B. R., Ilag, L. L., Rossmann, M. G., and Fane, B. A. (1996). Atomic structure of the degraded procapsid particle of the bacteriophage G4: Induced structural changes in the presence of calcium ions and functional implications. *J. Mol. Biol.* **256,** 736–750.

McKenna, R., Xia, D., Willingmann, P., Ilag, L. L., Krishnaswamy, S., Rossmann, M. G., Olson, N. H., Baker, T. S., and Incardona, N. L. (1992). Atomic structure of single-stranded DNA bacteriophage ΦX174 and its functional implications. *Nature* **355,** 137–143.

Mullineaux, P. M., Donson, J., Morris-Krsinich, B. A. M., Boulton, M. I., and Davies, J. W. (1984). The nucleotide sequence of maize streak virus DNA. *EMBO J.* **3,** 3063–3068.

Mullineaux, P. M., Boulton, M. I., Bowyer, P., Vandervlugt, R., Marks, M., Donson, J., and Davies, J. W. (1988). Detection of a non-structural protein of Mr 11000 encoded by the virion DNA of maize streak virus. *Plant Mol. Biol.* **11,** 57–66.

Palmer, K., and Rybicki, E. P. (1997). The use of geminiviruses in biotechnology and plant molecular biology, with particular focus on Mastreviruses. *Plant Science* **129,** 115–130.

Palmer, K., and Rybicki, E. P. (1998). The molecular biology of Mastreviruses. *Adv. Virus Res.* **50,** 183–234.

Pinner, M. S., Markham, P. G., Markham, R. H., and Dekker, E. L. (1988). Characterisation of maize streak virus: Description of strains and symptoms. *Plant Pathol.* **37,** 74–87.

Pitaksutheepong, C. (1999). Biological and functional aspects of the movement proteins of maize streak virus and bean yellow dwarf virus in transgenic plants. Ph.D. thesis, University of East Anglia, UK.

Rao, J. K. M. (1986). Sequence homology between the coat proteins of DNA and RNA plant viruses. *Biochem. Biophys. Res. Commun.* **134,** 372–377.

Simpson, A. A., Chipman, P. R., Baker, T. S., Tijssen, P., and Rossmann, M. G. (1998). The structure of an insect parvovirus (*Galleria mellonella densovirus*) at 3.7 Å resolution. *Structure* **6,** 1355–1367.

Thottappilly, G., Bosque-Perez, N., and Rossel, H. (1993). Viruses and virus diseases of maize in tropical Africa. *Plant Pathol.* **42,** 494–509.

Tsao, J., Chapman, M. S., Agbandje, M., Keller, W., Smith, K., Wu, H., Luo, M., Smith, T. J., Rossmann, M. G., Compans, R. W., and Parrish, C. R. (1991). The three-dimensional structure of canine parvovirus and its functional implications. *Science* **251,** 1456–1464.

Zhou, Z. H., Hardt, S., Wang, B., Sherman, M. B., Jakana, J., and Chiu, W. (1996). CTF determination of images of ice-embedded single particles using a graphics interface. *J. Struct. Biol.* **116,** 216–222.